Evidence for separate Mott and liquid-gas transitions in photoexcited, strained germanium

L. J. Schowalter,* F. M. Steranka, M. B. Salamon, and J. P. Wolfe
Physics Department and Materials Research Laboratory, University of Illinois at Urbana—Champaign, Urbana, Illinois 61801
(Received 11 March 1983)

The phase diagram of photoexcited electron-hole (*e-h*) pairs, which are confined to a strain well in stressed Ge, is investigated via measurements of energy spectra and spatial distributions of *e-h* recombination luminescence. From calculated fits to the energy spectra, we determined that the liquid-gas (LG) critical temperature was 4.5 ± 0.2 K. However, above 3.7 K, we observed excess luminescence between the typical free-exciton (FE) and *e-h*-liquid (EHL) lines. In addition, measurements of the actual spatial distributions of the *e-h* pairs indicate that sharp changes in density occur even at temperatures well above the measured LG critical temperature. We were able to quantitatively explain all of our data by assuming the presence of three phases separated by two phase transitions: a low-density FE gas separated by a Mott (metal-insulator) transition from an intermediate-density *e-h* gas (EHG) which in turn condenses into an EHL with still higher density. In this interpretation, the line of Mott transitions between the FE and EHG phases is determined to begin at a triple-point temperature of 3.7 ± 0.2 K and end at a critical point at 6.5 ± 0.5 K and density $(9\pm3)\times10^{15}$ cm^{-3}. A simple theory for the Mott transition gives a critical-point temperature of 5.4 K and density of 3.4×10^{15} cm^{-3}. Other interpretations of our data such as inhomogeneous strain broadening or the existence of excitonic complexes are considered but shown to be inadequate. However, the apparent small density difference between the FE and EHG phases makes it impossible to rule out the possibility that the Mott transition is actually continuous above the LG critical temperature. This last explanation is considered unlikely due to the temperature range over which the Mott transition is observed to remain sharp.

I. INTRODUCTION

A neutral Coulomb gas can be created in three dimensions by photoexciting high-purity semiconductors. At high temperatures, this gas will consist of equal numbers of uncorrelated electrons and holes. As the temperature is lowered, most of the charge carriers will associate into neutral bound pairs called free excitons (FE) if the gas density is sufficiently low. This low-temperature, insulating gas of hydrogenlike pairs will condense into a metallic electron-hole (*e-h*) liquid (EHL) if the density of the gas can be raised sufficiently. The EHL to Fe transition really involves two types of phase changes: a liquid-gas (LG) transition (generally, there is a large density difference between the two phases) and a metal-nonmetal transition commonly known as a Mott transition. As first proposed by Landau and Zeldovich[1] for expanded Hg, these two transitions, which appear to occur simultaneously at low temperatures, might actually separate into two distinct transitions at higher temperatures. However, none of the experimental work done on the phase diagrams of Hg and the alkali metals has demonstrated such a separation despite continued theoretical predictions of its feasibility.[2–4]

In this paper, we present experimental evidence for such a separation of the LG and Mott transitions of photogenerated electrons and holes in stressed Ge. We shall argue that strain confinement represents the best realization to date of a high-density, equilibrium phase and permits observation of the phase changes directly as volume changes, as well as through spectral features. Between 3.7 (triple point) and 4.5 K (LG critical point) a three-component spectrum [FE, EHL, and ionized *e-h* gas (EHG)] provides a consistent fit to the luminescence data. Further, coexistence of FE and EHG components can be followed to 6.5 K. Spatial analysis shows a volume change in the strain-confined carriers extending to 6.5 K—which we identify with the Mott transition line.

Photoexcited carriers in indirect band-gap semiconductors such as Si and Ge can have lifetimes much longer than their thermal relaxation times. Thus under appropriate conditions,[5] the finite lifetime of the electrons and holes may be neglected in calculating thermal equilibrium. However, the luminescence emitted by the eventual recombination of electrons and holes has proved useful in studying the different phases of the photoexcited Coulomb gas. Several such investigations[5–9] of photoexcited Ge and Si have attempted to explore the theoretical suggestions of Rice[10] and Combescot,[11] that the EHL critical density would be much higher than that of a Mott transition at the same temperature. However, experiments are not definitive and are subject to conflicting interpretation for reasons we discuss below.

Two principal experimental problems complicate the exploration of the EHL critical regime. First, it is quite difficult to produce the high density of photoexcited carriers necessary to reach the critical region. Second, it is difficult to know and control the density distribution of photoexcited carriers and the temperature profile of their host crystal. Most of the previous investigations[5–9] used

photoexcitation by laser radiation at photon energies above the semiconductor band gap so that all of the radiation was absorbed very near the crystal surface. This causes an EHG to be created near the surface whose density falls off in an ill-defined way toward the interior of the crystal. The density distribution is a complicated function of excitation spot size, intensity, and crystal temperature. At high excitation intensity, the inhomogeneous density distribution is complicated further by a inhomogeneous temperature distribution. Luminescence radiation is generally collected without spatial selection, and thus emanates from regions with large variations in the local *e-h* density and temperature. This makes it difficult to determine whether or not the observed changes in the spectrum are continuous functions of density and temperature.

Thomas and Rice[12] tried to avoid the problems of an inhomogeneous distribution of photoexcited carriers by photopumping a thin Ge crystal from both sides. However, they found that the densities of photoexcited *e-h* pairs, which they could maintain without excessively heating their sample, was an order of magnitude less than the LG critical density. This limit was likely the result of strong surface recombination which, along with carrier thermalization processes, produced high phonon densities which heated the liquid. Also, it is now well known[13] that phonon fluxes produce large forces on *e-h* droplets which would tend to push them out of the excitation region or into the crystal surfaces. To avoid significant heating of their sample, they limited their laser pumping power to less than 40 mW. Within the range of densities accessible to them, Thomas and Rice found no evidence for significant ionization of excitons. Instead, they were able to explain the observed broadening of the low-energy side of the exciton line in terms of small exciton complexes. Our results in stressed Ge show that the Mott transition occurs at densities very close to the LG critical density. Because stressing Ge changes both the degeneracies and masses of the electrons and holes, our results and those of Thomas and Rice cannot be directly compared. Our results do suggest, however, that higher densities must be obtained in unstressed Ge before it can be concluded that no separate Mott transition occurs in that system.

Clearly, a means of obtaining quasiequilibrium is necessary, and this requires the production of high densities of photoexcited carriers without significant heating of the Ge crystal. In our experiments, we used a strain-confinement scheme which meets the above requirements. An appropriate contact stress can be applied to Ge which will create a maximum uniaxial stress *inside* the Ge crystal, *away* from the crystal surface.[14] Since stress lowers the band-gap energy, the photoexcited carriers will be attracted to and confined within the region of maximum stress, which is commonly referred to as a strain well.

There are several distinct advantages in such a strain-confinement scheme. Since the strain well collects photoexcited carriers very efficiently and the carriers occupy a very small effective volume, high densities can be created at moderate pumping powers. For instance, we can typically observe the onset of condensation of EHL at 3 K at photoexcitation powers around 10 μW. In addition, there is no need to use a small Ge crystal, so higher photoexcitation powers can be used without significant heating problems. The strain well is surrounded by a large crystal, which provides an excellent heat sink. The strain well also greatly reduces the problems of recombination at surface traps by holding the carriers far away from the surface of the crystal. Decay at bulk traps is also reduced because the small volume of the well makes it possible to saturate a low density of such traps. This last point was demonstrated in a previous paper,[15] where exciton lifetimes of over 1 ms were observed in the strain well.

The density of *e-h* pairs is not uniform in the strain well, but is determined by the spatial variation of the band gap.[16] The variation of the density in the well is much easier to account for than the particle distributions normally produced by surface excitation, where the spatial distributions are determined by phonon winds,[13] particle mobilities, and lifetimes. When an approximate equation of state is known, as in the case of the FE gas, the density variation in the strain well can be calculated and incorporated into the analysis as shown in Sec. III. In the case of the *e-h* plasma (EHP), where the equation of state is less well known, a nearly homogeneous distribution can be achieved just above the threshold photoexcitation power, at which only a small amount of plasma condenses. Since the density of *e-h* pairs is greatest near the center of the strain well, this is where the plasma will first condense out of the FE gas. The strain gradients, which always accompany our confinement scheme, are minimal there and thus do not complicate the interpretation of the spectral data.

Another advantage of the strain-well geometry is that the density of photoexcited carriers can be determined directly from spatial measurements. Early work[14] using this technique showed that at low temperatures a single large *e-h* droplet is formed. Since the density of this droplet is determined from the spectral line shape of the luminescence, a measurement of the droplet size gives the total number of carriers in the strain well, which, in turn, allows us to determine densities directly from spatial measurements at higher temperatures. This technique is particularly important to our results since it provides, unlike previous investigations,[5–9] an *independent check* on the phase diagram calculated from spectral analysis of the recombination luminescence.

We report both the spectral content and spatial distribution of luminescence from the strain well as functions of temperature and laser power. The experimental spectra show qualitatively different behavior in four different temperature regions. In Sec. II, we first describe the experimental apparatus, and subsequently present our spectral data with associated line-shape analysis for each of the four temperature regions (Sec. III). The experimental phase diagram is presented in Sec. IV. The results of our spatial condensation measurements are described in Sec. V followed in Sec. VI by a theoretical calculation of the phase diagram. Finally, our conclusions are summarized in Sec. VII.

II. EXPERIMENTAL METHODS

Strain confinement of photoexcited carriers is the crucial element of the present study. An ultrapure crystal[17]

of dislocation-free Ge ($N_A - N_D \leq 2\times 10^{11}$ cm^{-3}) was stressed with a rounded nylon plunger, using the technique of Wolfe *et al.*[18] The crystal was photoexcited by a cw Nd:YAG (yttrium aluminum garnet) laser ($\lambda = 1.06$ μm). Measurements of the spatial extent of recombination luminescence were made by scanning a sharp image of the strain well across the entrance slit of a $\frac{1}{4}$-meter spectrometer. Infrared detection of the luminescence was accomplished with a high-sensitivity, cooled Ge photodiode. At low excitation levels, digital signal averaging was required.

The stressed sample was mounted in a flow-through optical cryostat provided with active temperature stabilization.[19] Either a Ge resistance thermometer, produced and calibrated by Cryo-Cal Inc., or a small carbon resistor, which we calibrated, was embedded in the OFHC copper block of the sample stresser for temperature measurement. Good control of the sample temperature was necessary since, near the phase boundaries, the recombination luminescence was very strongly temperature dependent. Our system was capable of controlling the average sample temperature over the period of an experimental scan (15 min or less) to better than 0.01 K.

In spectral measurements, the photoexcitation beam was modulated to allow phase-sensitive detection. We were concerned that this might cause modulations of the strain-well temperature at high photoexcitation powers to which our resistance thermometer would be insensitive. As described in an earlier publication,[15] the recombination luminescence of strain-confined excitons observed at constant photoexcitation power drops off exponentially with temperature. Thus by observing the time evolution of luminescence from excitons after the laser photoexcitation was turned on, we determined that for absorbed photoexcitation powers $P_{\rm abs}$ below 15 mW, the strain-well temperature modulation was sufficiently small (<0.1 K) to be acceptable. Most of our data were taken at lower powers since the strain well was very efficient in collecting the photoexcited carriers. However, in order to obtain liquid-like densities of *e-h* pairs at high temperatures, we used $P_{\rm abs}$ above 15 mW. In these cases, a temperature modulation of the strain well, in response to the modulation of the laser beam, became apparent. Spectra were taken by changing the duty cycle of our laser-beam modulator so that the sample was illuminated 80% of the time. We also used a low chopping frequency so that the photoexcited carriers in the strain well were in a steady-state equilibrium during most of the duty cycle. A boxcar integrator was then used to sample only the steady-state recombination luminescence. Of course, the actual temperature of the strain well was then systematically higher than that recorded by our resistance thermometer. However, this error is roughly estimated to be less than 0.2 K at the highest laser power we used ($P_{\rm abs} = 69$ mW).

TABLE I. The measured parameters for the three strain wells used in our experiments.

Strain well	α	E_0 (± 0.2 meV)
1	8.9 meV/mm^2	5.8 meV
2	not measured	5.4 meV
3	18 meV/mm^2	6.1 meV

Luminescence was collected through the crystal face opposite the excitation face. It is necessary to focus the excitation to a small spot and move this spot out of line with the center of the well in order to exclude luminescence from the surface near the excitation point. The light was passed through a bandpass interference filter with peak transmission at 1.65 μm. This filter was necessary for spatial-extent measurements of the energy-integrated recombination luminescence, and was also helpful in reducing background noise in spectral measurements.

As described in earlier work,[14] the rounded nylon stresser produces a shear-stress maximum, or band-gap minimum, inside the crystal. In our experiments a force of about 100 N (~ 10 kgf) applied to a 1-mm^2 contact area produced a spherical strain well located about 0.7 mm from the crystal surface, as observed by imaging the photoluminescence with an infrared vidicon. The strain-induced shift of the band-gap energy ΔE_g at small distances r from the center of the strain well is approximately

$$\Delta E_g = -E_0 + \alpha r^2 , \tag{2.1}$$

where E_0 is the maximum shift of the band gap and α characterizes the curvature of the strain well. E_0 was determined from the strain-induced shifts of the EHL emission, and α was found from the spatial extent of the exciton gas at low densities.[16] Our measurements were made on three different strain-well configurations which are described by the parameters listed in Table I.

III. LUMINESCENCE RESULTS

As mentioned in the Introduction, the luminescence spectra as a function of laser power show qualitatively different behavior in four temperature regions. In this section we describe each of the four regions and present the details of the line-shape analysis used to fit the spectra. We start at low temperatures where only FE and EHL are present and proceed to higher temperatures where the spectra are more complicated. All spectra presented here are LA phonon replicas since they are the most intense.

A. Region I: $T \leq 3.7$ K

At temperatures less than 3.7 K, all of the spectra could be fitted well using a convolution of EHL and FE line shapes only. The exciton line shape is given by

$$I_{\rm FE}(\epsilon) \propto \mathscr{D}_x^{\rm SW}(\epsilon - E_x^{\rm BB}) \exp[-\beta(\epsilon - E_x^{\rm BB})] , \tag{3.1}$$

where ϵ is the photon energy and $E_x^{\rm BB}$ is the FE band-bottom energy. We calculate the appropriate density of states, $\mathscr{D}_x^{\rm SW}$, for an exciton in the strain well by observing that its energy is

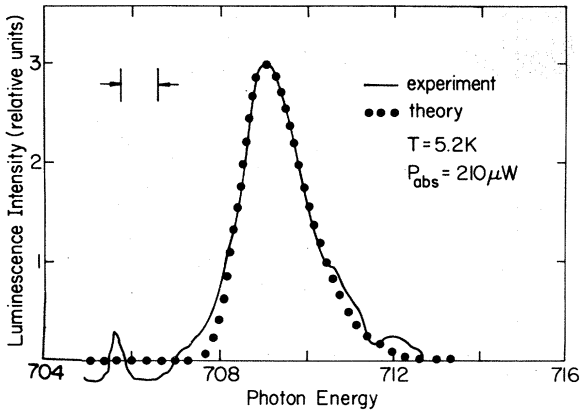

FIG. 1. Measured intensity of FE recombination luminescence vs photon energy is shown as a solid line. This is the LA phonon replica as are all spectra presented in this paper. The solid circles were calculated by fitting with only two free parameters (position and amplitude) as explained in the text. The calculated line shape here, as in all the other fits presented, was broadened by a triangle resolution function whose width is indicated in the figure. This width, which is about 20% greater than the theoretical resolution of our spectrometer, was due to broadening from our electronic signal processing.

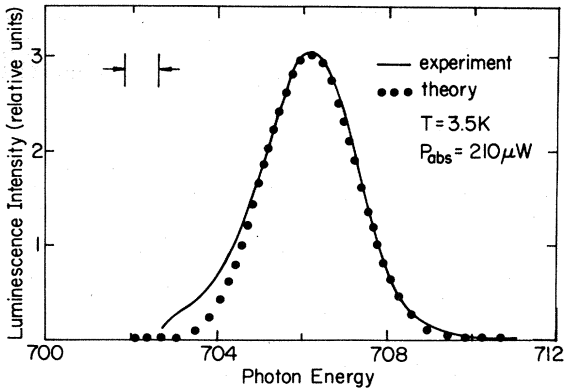

FIG. 2. Solid line is the measured luminescence intensity vs photon energy under conditions in which most of the photoexcited carriers in the strain well have condensed into an EHL. The solid circle represents a fit to the EHL luminescence calculated with three free parameters: position, amplitude, and the density of the EHL which determines the width of the line shape. The EHL density and the band-bottom energy were determined to be 4.4×10^{16} cm^{-3} and 703.1 meV, respectively.

$$\epsilon_x=\frac{p^2}{2m_{dx}}+\alpha r^2+E_x^{\mathrm{BB}}\,, \tag{3.2}$$

where p is its momentum, m_{dx} is its density-of-states mass, and r is the distance of the exciton from the center of the well. For a band-gap shift $E_0>2$ meV, the density-of-states mass approximation for excitons in uniaxially stressed Ge is expected to be quite good.[20] For convenience we define $\epsilon'=\epsilon-E_x^{\mathrm{BB}}$. The density-of-states function will then be

$$\begin{aligned}\mathscr{D}_x^{\mathrm{SW}}(\epsilon')d\epsilon'&=(2\pi\hbar)^{-3}\int_{\epsilon'}^{\epsilon'+d\epsilon'}d^3r\,d^3p\\&=\nu_x\frac{G}{2}\left[\frac{m_{dx}}{2\pi^2\hbar^2\alpha}\right]^{3/2}\epsilon'^2d\epsilon'\,,\end{aligned} \tag{3.3}$$

if $\epsilon'>0$; otherwise, $\mathscr{D}_x^{\mathrm{SW}}(\epsilon')=0$. The constant G is a geometrical factor equal to the surface area of a six-dimensional sphere of unit radius, and ν_x is the degeneracy of exciton states. This density of states for strain-confined excitons has also been derived by Gourley and Wolfe[16] from a somewhat different point of view. Note that $\mathscr{D}_x^{\mathrm{SW}}$ already takes into account the spatial variation of the FE density due to the strain gradients of the well. A fit to an exciton line shape using the ϵ'^2 density of states is shown in Fig. 1. The theoretical line shape was broadened by a triangular resolution function whose width is indicated in the figure. The same resolution function was used in calculating all fits. Position (determined by the energy E_x^{BB}) and intensity are the only fitting parameters used. The linewidth is independent of the FE density since the excitons obey Maxwell-Boltzmann (MB) statistics.

The line shape for an EHL of uniform density is given by the usual convolution of the electron and hole density of states,[5]

$$\begin{aligned}I_{\mathrm{EHL}}(\epsilon,E_{\mathrm{EHL}}^{\mathrm{BB}})\propto\int d\epsilon_e\mathscr{D}_e(\epsilon_e)f(\epsilon_e-\mu_e)\\\times\mathscr{D}_h(\epsilon-E_{\mathrm{EHL}}^{\mathrm{BB}}-\epsilon_e)\\\times f(\epsilon-E_{\mathrm{EHL}}^{\mathrm{BB}}-\epsilon_e-\mu_h)\,,\end{aligned} \tag{3.4}$$

where $f(x)=(e^{\beta x}+1)^{-1}$ is the Fermi function, $\beta=(k_BT)^{-1}$, μ_e and μ_h are the chemical potentials for the electrons and holes, $\mathscr{D}_e$ and $\mathscr{D}_h$ are the respective density-of-states functions, and $E_{\mathrm{EHL}}^{\mathrm{BB}}$ is the EHL band-bottom energy. The electron density of states was approx-

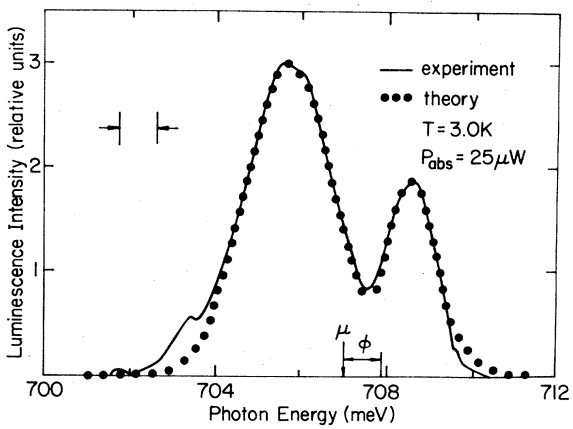

FIG. 3. Luminescence spectrum (solid line) taken under conditions in which the recombination intensities from the EHL and FE phases are approximately equal. The solid circles were calculated with five free parameters as discussed in the text. From this fit, the EHL density and band-bottom energy were determined to be 4.4×10^{16} cm^{-3} and 702.7 meV, respectively. The chemical potential μ of the EHL-FE system was found to be 707.0 meV and EHL binding energy ϕ was equal to 0.87 meV.

imated with a density-of-states mass $m_{de}=0.22m_e$, and the strain-induced splitting of the conduction-band minima was taken into account. The stress-dependent hole density of states was determined from the tabulations of Kelso.[21] A typical fit to a spectrum in which recombination luminescence from the EHL dominates is shown in Fig. 2. This fit requires three free parameters: the amplitude, the position of the low-energy edge ($E_{\rm EHL}^{\rm BB}$), and the chemical potential, $\mu=\mu_e+\mu_h+E_{\rm EHL}^{\rm BB}$, which determines the width of the line. The electron and hole chemical potentials, μ_e and μ_h, from which the electron and hole densities can be determined,[5] are not independent since charge neutrality requires the two densities to be equal.

At somewhat lower photoexcitation powers it is possible to resolve luminescence from both the FE and EHL components simultaneously, as shown in Fig. 3. This fit used five free parameters: two are associated with the FE line and three with the EHL line as described above. In addition to the EHL density, the FE density can also be determined from such a fit. This is possible because the chemical potential of the FE must be the same as the EHL with which they are in thermal equilibrium. Now the liquid binding energy ϕ, which is the difference between the low-energy edge of the FE luminescence and μ, can be used to determine the FE density at the LG interface,[5]

$$n_x(T)=e^{-\phi/k_BT}\int_0^\infty e^{-\epsilon/k_BT}\mathscr{D}_x(\epsilon)d\epsilon\,, \tag{3.5}$$

where

$$\mathscr{D}_x(\epsilon)d\epsilon=\frac{\nu_x m_{dx}^{3/2}\epsilon^{1/2}}{\sqrt{2}\pi^2\hbar^3}\,, \tag{3.6}$$

is the local density of states for excitons. For our case,[22] $\nu_x=4$ and $m_{dx}=0.415m_e$. From the fit shown in Fig. 3, we find the EHL density $n_{\rm EHL}(3\ {\rm K})=4.4\times10^{16}\ {\rm cm}^{-3}$ and the EHL binding energy $\phi(3\ {\rm K})=0.87$ meV. The corresponding exciton density at 3 K is $4.8\times10^{14}\ {\rm cm}^{-3}$. In the above analysis we neglect the contribution of the strain well, which varies with position as αr^2, to the chemical potential. This approximation is valid if the radius R of the EHL sphere is sufficiently small so that $\alpha R^2\ll\phi$. From spatial measurements discussed in Sec. V, we found $R<100\ \mu$m under the same excitation conditions used for the spectrum shown in Fig. 3. Thus the above inequality is satisfied.

The behavior of the spectra in this temperature region as a function of laser power is shown in Fig. 4. At low laser powers ($<10\ \mu$W) only FE are present (not shown). As laser power is increased, the intensity of the FE line increases up to a threshold level[23,24] above which luminescence from the EHL appears abruptly, and soon dominates the spectrum since its density is much higher than that of excitons. Note that the position of the low-energy edge and the width of the EHL line shape is nearly independent of laser power. Since both of these parameters depend sensitively on the liquid density, this implies that the EHL density remains fixed in the power range shown in Fig. 4. At very high powers, the liquid density does increase slowly with power, due to compression of EHL by the strain gradients in the well[25] as its volume increases.

B. Region II: $3.7<T<4.6$ K

At temperatures above 3.7 K it is no longer possible to fit the spectra using only FE and EHL components. Considerable excess luminescence arises between the two peaks. An example of such a spectrum is shown in Fig. 5. We considered several different models for this extra luminescence including compression broadening of the EHL line shape, the presence of biexcitons and other multiexciton complexes, and the appearance of an EHG. As we now describe, only the EHG model can consistently explain all of our data. First, we discuss the spectral features expected from the various models.

As was mentioned, the position of the low-energy edge of an EHP line shape is density dependent. We have cal-

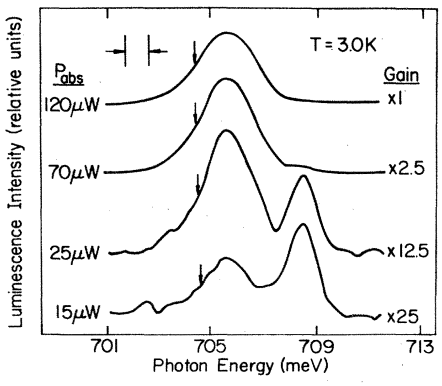

FIG. 4. Luminescence intensity vs photon energy is plotted for four different photoexcitation powers $P_{\rm abs}$. All spectra were taken at the same temperature ($T=3$ K). The arrows indicate the photon energy at which the intensity has dropped to one-half of its peak value. Note that the position of this arrow on the low-energy side of the peak does not change with increasing $P_{\rm abs}$ at this temperature.

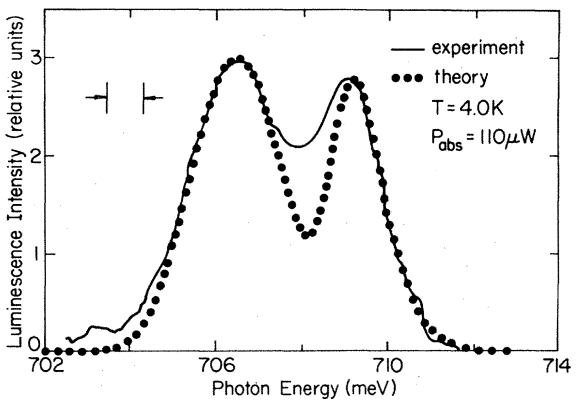

FIG. 5. Best possible fit (solid circles) using only an EHL and FE replica to a recombination luminescence spectrum (solid line) at 4 K is displayed. Considerable excess luminescence is left unfitted between the calculated FE and EHL lines. The EHL replica can be made broader by considering the liquid to be compressed. However, as explained in the text, the densities of EHL required to make the replica broad enough also shift the low-energy edge of the replica to much lower energies than actually observed.

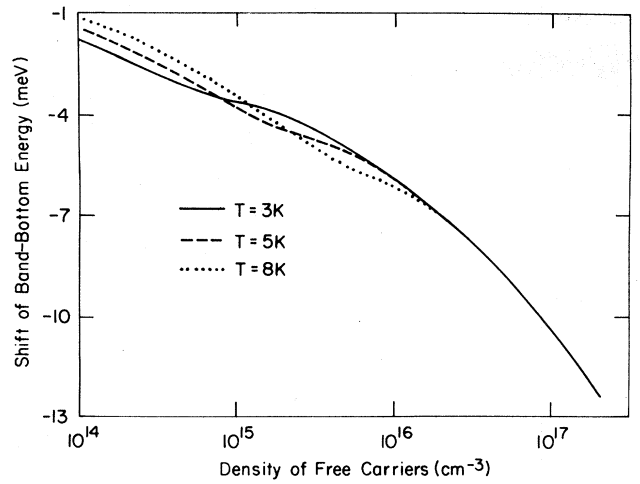

FIG. 6. Density dependence of the band-bottom energy is shown for several temperatures. These curves were generated by interpolating between the high-density calculations of Vashishta *et al.* (Ref. 26) and the low-density calculations of Zimmerman *et al.* (Ref. 27). The method of interpolation, which was purely phenomenological, is explained in the Appendix.

culated the density dependence of this "band-bottom energy," $E_{BB}(n,T)$, for the density range of interest by interpolating between the calculations of Vashishta *et al.*[26] and Zimmerman *et al.*[27] The former calculation is expected to be accurate when the plasma is degenerate, and the latter at low densities where the plasma obeys MB statistics. The resulting band-bottom shift, plotted as a function of density at several different temperatures, is shown in Fig. 6. Our interpolation technique is described in the Appendix. Given the band-bottom shift as a function of density, we can eliminate E_{EHL}^{BB} as one of the parameters in the liquid line-shape fits, once the position of the low-energy edge and density of one liquid peak is determined. We used the fit shown in Fig. 3 to fix $E_{BB}(n=4.4\times10^{16}$ cm^{-3}, $T=3$ K$)=702.7$ meV. This elimination of a free parameter was important in the interpretation of fits to high-temperature spectra as will be described later in this section.

Knowing $E_{BB}(n,T)$ also enabled us to eliminate compressional broadening of the EHL line shape as a possible explanation of the excess luminescence. The line shape I'_{EHL} for luminescence from a sphere of EHL whose density n varies with radius r can be calculated as

$$I'_{EHL}(\epsilon)\propto\int_0^R r^2 n(r)\rho(n)I_{EHL}(\epsilon,E_{BB}(n))\,, \tag{3.7}$$

where R is the radius of the EHL sphere, $I_{EHL}(\epsilon,E_{BB}(n))$ is the line shape calculated with Eq. (3.4) for a uniform density plasma, and $\rho(n)$ is the relative enhancement factor as a function of density. We took[28] $\rho(n)\propto n^{2/3}$, although we found little difference in the calculated line shape when we tried $\rho(n)\propto n$. The EHL density distribution was approximated by assuming that the increase in EHL density near the center of the strain well would be proportional to the increase in pressure. In this case, the EHL density will increase with distance as[21,25,29]

$$n(r)=n+K(R^2-r^2)\,, \tag{3.8}$$

where K is left as a fitting parameter. Once the position in energy of the compressed line shape was eliminated as a free parameter, we found that it was impossible to make the line shape sufficiently broad to fit the spectrum and still have it located in the correct spectral position. In fact, line shapes calculated for large values of K, with Eqs. (3.7) and (3.8), were close to EHL line shapes calculated for uniform spheres of high-density liquid. This apparent uniformity results because the luminescence is dominated by the high density of e-h pairs near the center of the strain well. We conclude that the observed excess luminescence could not be due solely to compressional effects.

We also considered biexcitons and other excitonic complexes as the source of the excess luminescence. Three experimental facts are inconsistent with such an explanation. (i) The excess luminescence appears abruptly as laser power is increased—more rapidly than can be explained by the entropy-controlled associations of excitons into complexes. (ii) The width in energy of the excess luminescence is too narrow. (iii) Our spatial scans show that as temperature is lowered (keeping laser power constant), the spatial distribution of the strain-well luminescence shrinks rapidly over a narrow temperature region. At low temperature, this spatial contraction coincides with EHL condensation as determined by the spectral measurements. However, rapid spatial condensation also occurs at temperatures well above the EHL critical temperature. Such a condensation is not expected for excitonic complexes, but can be explained by the presence of an EHG.

The measured spectra can be fitted with an EHG component as the source of the excess luminescence. The line shape given by Eq. (3.4) was used, but with values of μ_e and μ_h much smaller than those used to generate the EHL line shape. An example of such a three-component fit is shown in Fig. 7. As the liquid peak is not clearly resolved, we used its low-energy edge and our calculated $E_{BB}(n,T)$ to fix the density and, hence, the chemical po-

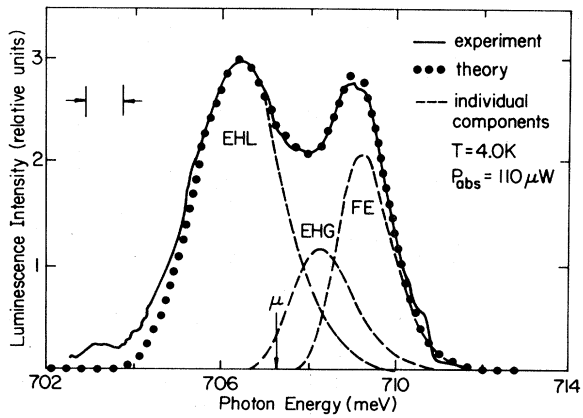

FIG. 7. Same luminescence spectrum (solid line) shown in Fig. 5 has been refitted with a line shape (solid circles) calculated using three components (dashed lines): FE, EHL, and EHG. The chemical potential μ of the three-component system, as determined from the fit, is indicated in the figure.

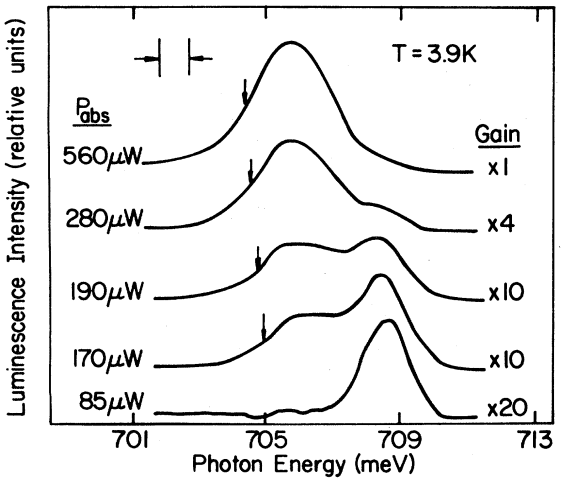

FIG. 8. Series of spectra taken at 3.9 K for different absorbed photoexcitation power P_{abs}. Note that, as in the series of spectra measured at 3.0 K shown in Fig. 4, the low-energy edge of the EHL luminescence is not very sensitive to increasing photoexcitation power. This is indicated by the fact that the arrows, which indicate the energy at which the intensity has dropped to one-half of its peak value, remain almost constant as P_{abs} increases. All the spectra in this figure can be fitted with a combination of EHL, EHG, and FE line shapes by keeping the spectral position of each component fixed and changing only their relative intensities.

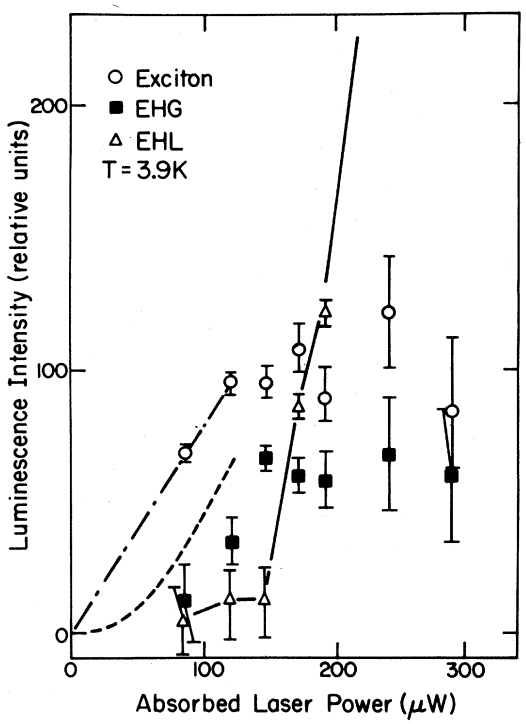

FIG. 9. Peak intensities of the EHL, EHG, and FE components are plotted as a function of adsorbed photoexcitation power P_{abs} at 3.9 K. These intensities were determined by fitting measured luminescence spectra, including those shown in Fig. 8, with the three components. In this series of fits, only the relative intensities of the three components were varied. The FE component increases with laser power until $P_{abs} \simeq 120$ μW, at which point luminescence from the EHG component appears. At higher photoexcitation powers, the intensity of the FE component remains almost constant. On the other hand, the EHG-component intensity increases rapidly until it also saturates at about 150 μW, which is the onset excitation power for the EHL. Note that the EHG intensity appears abruptly and grows more rapidly than the square of the FE intensity, contrary to the results expected if the excess luminescence were due to the formation of biexcitons. This is shown in the figure as a dashed line which was normalized by noting that, at the saturated FE intensity, the biexciton intensity should also remain constant.

tential of the liquid. Now, since the EHL and EHG are in equilibrium along their common interface, their chemical potentials must be equal. This fixes the density of the EHG and, thus, the spectral width of its luminescence. With these constraints, only six free parameters remain: the spectral positions and intensities of the EHL, EHG, and FE lines. The densities determined in this manner from the fit shown in Fig. 7 are $n_{EHL}(4.0\ \text{K}) = 3.1 \times 10^{16} \text{cm}^{-3}$ and $n_{EHG}(4\ \text{K}) = 2.3 \times 10^{15}\ \text{cm}^{-3}$. Note the width in energy of the EHG luminescence is much narrower than that due to the EHL which is opposite the result expected for excitonic complexes.[12]

Using $E_{BB}(n,T)$ again, we can independently determine the density of the EHG from its low-energy edge. This yields $n_{EHG}(4.0\ \text{K}) = 2.7 \times 10^{15}\ \text{cm}^{-3}$. While this result is approximate due to the uncertainty in determining E_{BB}, it agrees well with the density values found from equating the EHG and EHL chemical potentials, providing strong evidence for the EHG interpretation.

A typical power dependence in this temperature range ($3.7 < T < 4.6$ K) is shown in Fig. 8. Once again, the low-energy edge of the luminescence is not sensitive to laser power for a range above the liquid threshold. This indicates that the critical temperature of the liquid has not yet been reached; the liquid density is still fixed by a phase boundary. However, as before, sufficiently high photoexcitation powers will create enough EHL in the strain well so as to compress the liquid in the center with a subsequent red shifting of the EHL's low-energy edge.

We can fit each of the spectra shown in Fig. 8 with a convolution of EHL, EHG, and FE line shapes, keeping their spectral positions fixed and changing only their relative intensities. The intensity of each component is plotted versus laser power in Fig. 9. The intensity of the EHG exhibits an abrupt onset and grows more rapidly than the square of the FE intensity (the law expected if the excess luminescence were due to the formation of biexcitons).[30] The FE intensity saturates when the EHG starts to form, and the EHG intensity saturates once EHL starts to condense. We will discuss this intensity plot in terms of the phase diagram in Sec. IV.

C. Region III: $4.6 < T < 6.5$ K

Above 4.6 K the low-energy edge of the luminescence is quite sensitive to laser power, as can clearly be seen in Fig. 10. The low-energy half-intensity position moves by ~1.0 meV when P_{abs} changes from 590 to 730 μW (only 25%

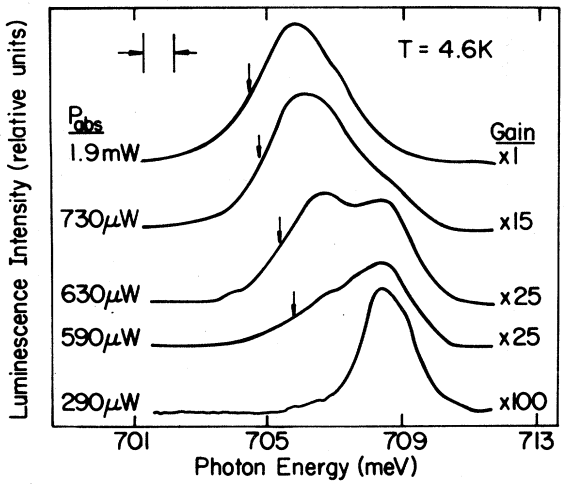

FIG. 10. Series of luminescence spectra taken at 4.6 K. Once again, the arrow indicates the photon energy at which the luminescence intensity of the EHL has decreased to one-half of its peak value. Note here, however, that the low-energy edge of the EHP luminescence is quite sensitive to photoexcitation power as explained in the text.

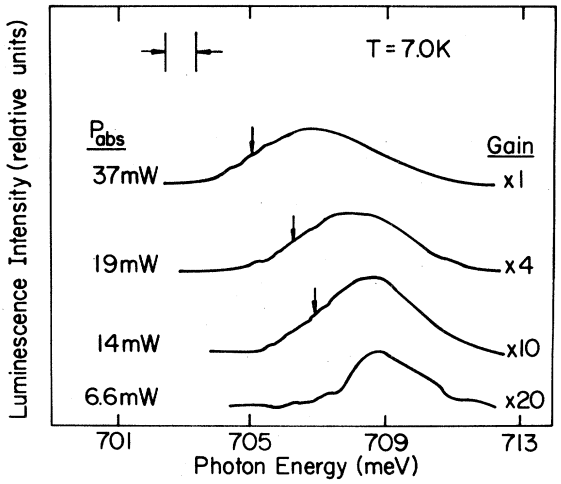

FIG. 12. Four luminescence spectra measured at 7.0 K for varying photoexcitation powers are shown. Note that the spectra change continuously from being FE-like at 6.6 mW to an EHP appearance at 37 mW.

change in power). This indicates that 4.6 K is very near or above the EHL critical temperature T_{LG}. The liquid density is no longer fixed by a phase boundary, and the transition between the EHL and EHG phases is continuous.

In this temperature range, the system's chemical potential could no longer be determined by fitting the EHL line. Hence the spectra were fitted to make the density of the EHG consistent with that determined from the position of its low-energy edge. These two-component (EHG and FE) fits to the spectra were not particularly good as substantial low-energy luminescence was left unfitted. Most of this low-energy luminescence is probably due to the compressional effects of the strain well. As will be explained in Sec. IV with the help of a phase diagram, the EHP is expected to be particularly sensitive to these effects in the supercritical regions at temperatures above T_{LG}. Unfitted luminescence may also be due in part to many-body effects which are neglected in the EHG line shape or to excitonic complexes. In any case, the major portion of the luminescence intensity was fitted by the two calculated peaks.

Considerable uncertainty in choosing the EHG spectral position (and hence density) in this temperature range makes it impossible to obtain definite values for the EHG density. We were able, however, to place upper bounds on the EHG density from the luminescence fits by moving the EHG peak to the lowest-possible energy that still gave a good fit to the high-energy edge. Since this procedure requires an increase in density as the peak is moved to lower energy, it gives reasonable upper bounds for the EHG density, but leaves the lower bounds undetermined. An example of such a fit is shown in Fig. 11. The upper bound for the EHG density at 5.4 K was determined from this fit to be $n_{max}\mathrm{EHG}(5.4\ \mathrm{K}) = 9.2\times10^{15}\ \mathrm{cm}^{-3}$.

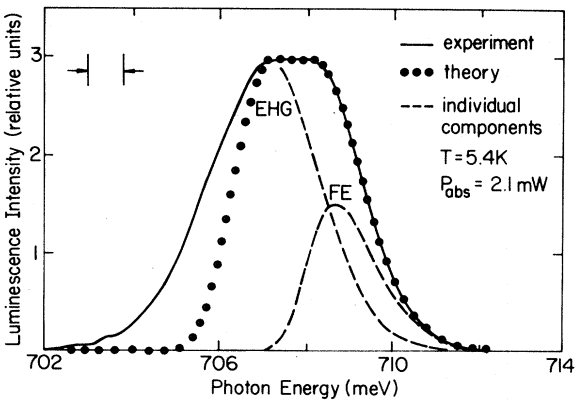

FIG. 11. Luminescence spectrum measured at 5.4 shown as an example of our fitting procedure in the temperature range $4.6 < T < 6.5$ K. Substantial low-energy luminescence was left unfitted; most of this is probably due to EHP compressed by the strain inhomogeneity of the strain well. However, as explained in the text, it was inappropriate to introduce an EHL component as the low-energy edge of the luminescence varied substantially with small changes in P_{abs}.

D. Region IV: $T > 6.5$ K

Above 6.5 K, the spectra no longer have a two-peak appearance; the luminescence peak shifts continuously from being FE-like at low excitation levels to being EHG-like at higher excitation levels, as demonstrated in Fig. 12. Attempts to fit these spectra using EHG and FE line shapes (as was done in the previous temperature range) gave upper bounds on the EHG density smaller than the exciton density determined from the spatial data. Therefore, we have assigned the Mott-transition critical temperature to be 6.5 K.

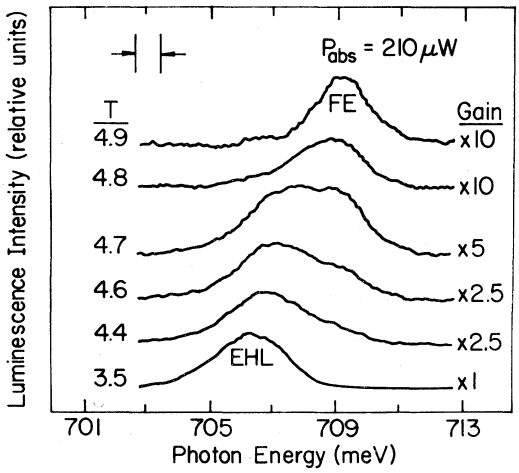

FIG. 13. Series of spectra for which the absorbed laser power was kept fixed at 210 μW and the temperature of the Ge sample was changed. At low temperatures, most of the luminescence from the strain well comes from the EHL component, while at high temperatures only FE remain. In the transition region, two peaks were observed since the luminescence intensities from the two components were comparable.

E. Other general features

Several other general features of the spectral data are revealed when laser power is kept fixed and the temperature is changed. A typical set of such spectra is shown in Fig. 13. At low temperatures, the spectrum is dominated by recombination luminesence from the EHL; FE are present far out in the strain well, but their density is much lower. As the temperature is increased, the density of FE coexisting with the EHL increases and thus their relative intensity also increases. Note that at this absorbed photoexcitation power $P_{abs}=210$ μW, there is a very narrow temperature range (4.6–4.7 K) where there are two distinct spectral peaks. As the temperature is raised, the low-energy EHL peak appears to shift toward higher energy and decrease in intensity as the EHG luminescence grows. For simplicity in the following analysis, we label the EHL-EHG peaks as EHP or "plasma."

We have plotted the spectral position of the two peaks as functions of temperature at several different laser powers in Fig. 14. For laser powers below about 5 mW, the transition between the EHP and FE occurs below 6.5 K and the temperature regime where both peaks were simultaneously observed was very narrow. At higher powers, the narrow two-peak region was not observable, and the EHP peak gradually shifted to the FE energy. We interpret this to mean that the FE-to-EHP transition is first order up to about 6.5 K. This temperature is well above the LG critical temperature which, from previously presented data, is estimated to be at 4.5 K.

Note also in Fig. 14, that the exciton peak position shifts with temperature even above the transition. We have plotted the peak position of the FE replica, measured well below the EHL condensation threshold, versus temperature in Fig. 15. From Eq. (3.3) we expect the FE peak

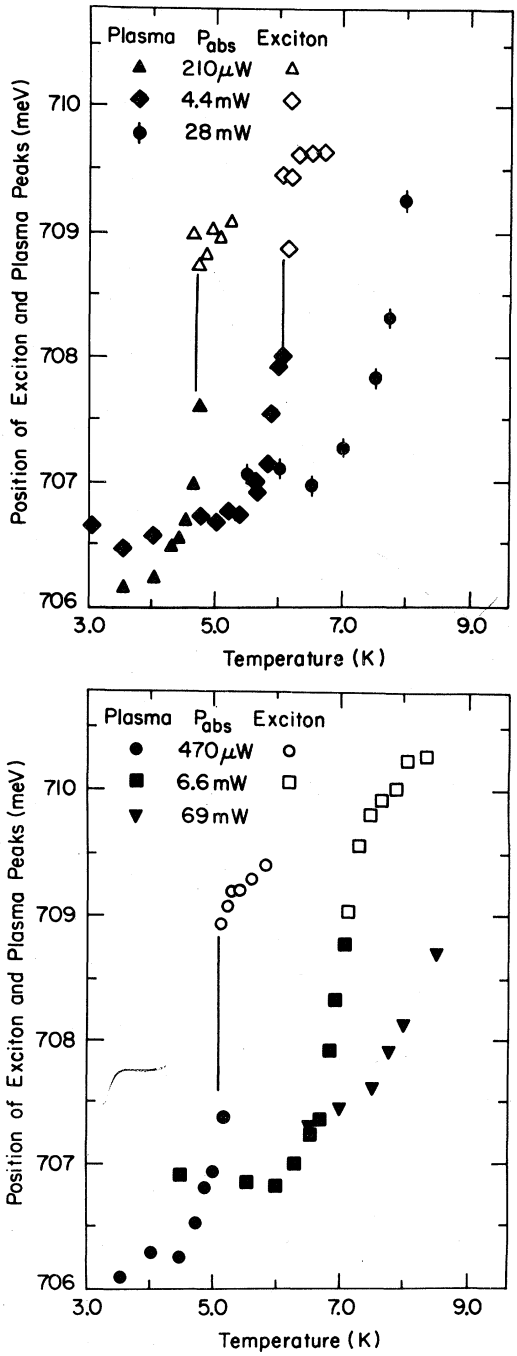

FIG. 14. Spectral position of the FE and EHP peaks plotted vs temperature. Each of the six series of spectra shown were made at constant photoexcitation power while the temperature was varied. The transitions between plasma and FE (which are indicated in the figure by solid squares) occur at increasingly higher temperatures as the photoexcitation power is increased. Above 6.5 K, it was no longer possible to resolve a discontinuity in the spectra as the transition from plasma to exciton was made.

position E_p to vary with temperature as

$$E_p=2k_BT+E_0=0.17T+E_0\ , \tag{3.9}$$

where E_0 is a constant in units of meV and T is measured

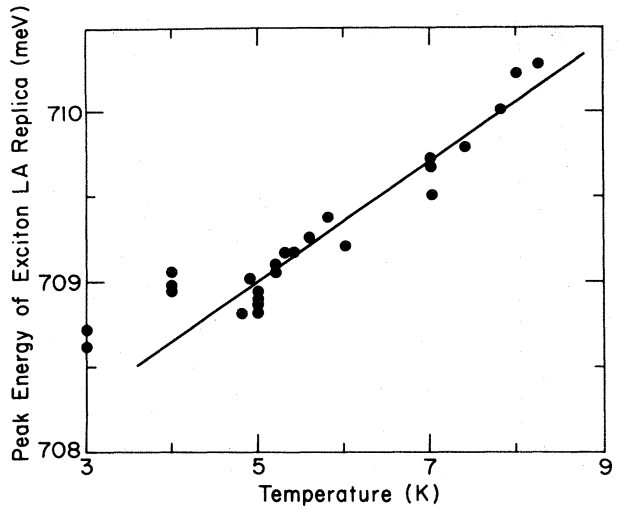

FIG. 15. Peak position in energy of the FE luminescence vs temperature. These spectra were measured at photoexcitation powers well below the EHP condensation threshold. The solid line shown is a straight-line fit to the data with slope 0.35 meV/K. As noted in the text, this is much steeper than theory would predict.

in K. However, the slope of the solid line in Fig. 15 is 0.35 meV/K. This difference cannot be explained by the band gap's temperature dependence, since it is very small at these low temperatures and in the opposite direction. This anomalous temperature dependence of the FE spectral position is not understood.

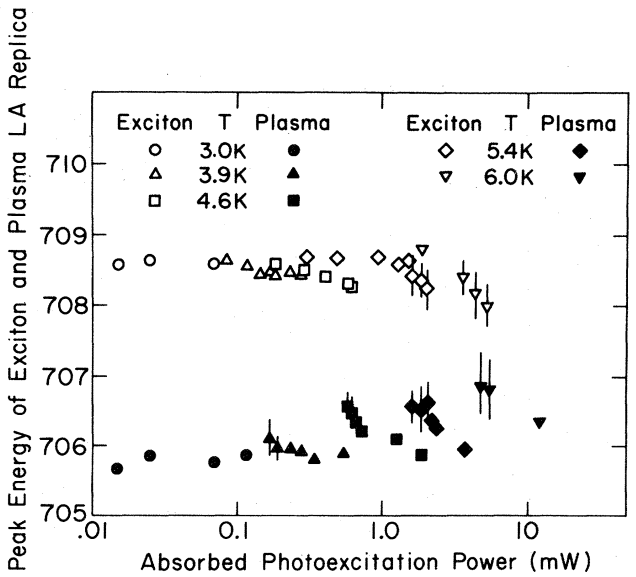

FIG. 16. Position, in photon energy, of the peak intensity of the FE and EHP replicas is shown vs P_{abs} at constant temperature. The error in measuring the peak position is indicated by a vertical line; otherwise, it is the same magnitude as the symbol size. Note that the range of powers over which both peaks can be resolved falls off sharply above 4 K. Measurements made at different temperatures were made in slightly different strain wells. Thus the peak positions of different temperature runs should not be compared.

In Fig. 16 we have plotted the FE and EHP positions as a function of laser power (and therefore average carrier density) along several isotherms. Below the triple point (3.7 K) the peak positions are insensitive to pumping power and temperature change. Above the critical point (4.5 K), however, the EHP peak position becomes strongly dependent on power, with a strong shift over a narrow range of photoexcitation. At temperatures higher than those shown in Fig. 16, only a single broad line shape is observed. Since the strain-well parameters were slightly different at different temperatures, the peak positions are also slightly shifted.

IV. PHASE DIAGRAM

The luminescence results presented in the preceding section permit us to determine (i) the EHL and FE densities along the coexistence curve up to 3.7 K, (ii) the coexisting EHL and EHG densities between 3.7 and 4.5 K, and (iii) upper bounds on the EHG density for $4.5 \leq T < 6.5$ K. To map out the rest of the phase diagram, we need to determine the exciton densities for temperatures above 3.7 K.

To do this we note that the intensity of the FE luminescence I_{FE} is proportional to the total number of excitons N_x in the well. Now, the excitons in a strain well behave as a classical gas in a parabolic potential, and thus their density distribution is given by

$$n_x(r) = n_{x0} \exp(-\beta \alpha r^2) , \tag{4.1}$$

where $\beta = (k_B T)^{-1}$, α is the well parameter, r is the distance from the center of the well, and $n_{x0} = n_x(0)$. Thus integrating Eq. (4.1) over all space, N_x is related to the density at the center of the well by

$$N_x \propto T^{3/2} n_{x0} \propto I_x . \tag{4.2}$$

If the well is filled just to the threshold for EHL condensation at each temperature, one can determine the density relative to a reference temperature T_r by

$$n_{x0}(T) = T_r^{3/2} I_x(T) / T^{3/2} I_x(T_r) .$$

This method has also been used by Furneaux[23] for strained Ge at low temperatures. We use our spectroscopic determination of ϕ at 3 K and Eq. (3.3) to get $n_{x0}(3\text{ K}) = 4.8 \times 10^{14}$ cm^{-3}. Values obtained in this way are plotted as the solid circles on the phase diagram shown in Fig. 17. The EHL and EHG densities determined from spectral fits to the luminescence data are shown as open circles. Above 4.5 K, the upper bounds determined for the EHG densities are shown as ◂▸. We have estimated the triple-point temperature (the temperature at which FE, EHL, and EHG coexist) to be 3.7 ± 0.2 K, and the critical temperatures of the LG and Mott transitions to be 4.5 ± 0.2 and 6.5 ± 0.5 K, respectively.

The shift of the single luminescence peak from FE to EHP position still occcurs rapidly at temperatures above 6.5 K as laser power is increased. However, no distinct coexistence region can be found. We interpret this to be a

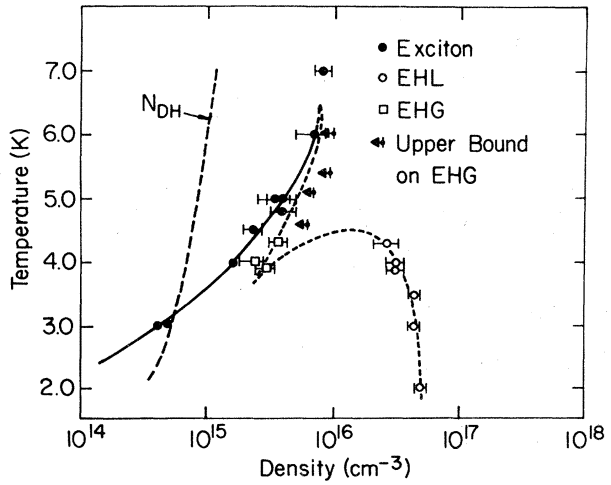

FIG. 17. Phase diagram of the exciton-EHL-EHG system in strained Ge on a temperature vs density plot. The points shown are the experimentally determined densities of the components at the phase boundaries as explained in the text. Density error bars are indicated unless they are smaller than the symbol used. The ◂▸ symbols, used for the EHG densities at 4.6 K and above, only represent upper bounds on the EHG density at the transition. We were unable to place lower bounds on the EHG density in this temperature range. The solid line represents exciton densities at the phase boundary calculated by Eq. (3.5) using a constant value for the liquid binding energy, $\phi=0.87$ meV, which was measured at 3 K. The dashed line on the high-density side of the phase diagram indicates the approximate position of the phase boundary based on the data points. The classical DH density N_{DH} for the metal-insulator transition vs temperature is indicated as a dashed line. The density N_{DH} is defined in Eq. (A8) in the Appendix.

transcritical region in the phase diagram, just above the Mott critical temperature. The exciton density near this transition at 7.0 K is also shown on the phase diagram.

The dashed line in Fig. 17 indicates the density at which classical Debye-Hückel (DH) screening theory predicts the ionization of the FE into an EHP. Note that we do not observe the Mott transition until much higher densities. This observation is in agreement with the work of Thomas and Rice[12] who also found no Mott transition even at densities significantly above the DH density. This was attributed to quantum corrections to classical DH theory, as originally suggested by Kremp *et al.*[31] We will compare this phase diagram with theoretical estimates in Sec. VI.

A disadvantage of strain-well confinement is that there is always a density gradient induced by the potential. This gradient can result in the existence of one or two interfaces in the well. When the temperature is below the triple point, only one interface, between EHL and FE, can exist, and its distance from the center will depend on the number of carriers in the well (i.e., on pumping power). Between the triple point and the critical point, two interfaces will be found: between EHL and EHG and between EHG and FE. The small density differences between the FE and EHG, as determined spectroscopically, would indicate that the distance between the two interfaces will be small. Between the LG and Mott critical points there is again only a single interface separating FE and EHG phases. Finally, above the Mott critical point there are no separate phases.

In the region where the three phases can coexist, we expect a core of EHL, with a relatively constant density owing to its low compressibility, surrounded by a narrow shell of more compressible EHG, and an atmosphere of FE extending to much larger radii. The sequence of events in Fig. 9 can now be understood. These data were taken at fixed temperature in the three-phase region. At low power, the density at the center of the well is below the phase boundary, and the number of excitons increases linearly with laser power. Near 100 μW, a core of EHG forms and grows rapidly as the number of carriers is increased, while the number of excitons stays fixed. Near 200 μW, an EHL drop begins to condense and all further carriers added increase the size of the EHL component. Because of its greater density, the EHL luminescence quickly dominates the spectrum. In the next section we describe the spatial results which corroborate this picture of the structure of the condensed phases in a strain well.

V. SPATIAL CONDENSATION MEASUREMENTS

As noted in the Introduction, the strain well allows us to determine the density of the confined carriers by measuring the volume they occupy, a unique advantage. As previously described, the spatial extent of recombination luminescence was determined by passing a sharply focused image of the strain well across the entrance slit of our photodetector.[18] The measurements were generally made without energy resolution in order to measure lower intensities than would have been possible otherwise. All measurements reported here were from a strain well with $\alpha=8.9$ meV/mm^2. While qualitatively similar results were obtained from other strain wells with larger α, the results were more difficult to interpret, due to the difficulty in resolving the FE signal in narrower strain wells.

Two typical spatial scans are shown in Fig. 18. In both cases, spectral measurements showed only FE to be present in the strain well under these conditions. The circles in Fig. 18 are determined from Eq. (4.1) using $\alpha=8.9$ meV/mm^2 and, as can be seen from the figure, the agreement is rather good. This Gaussian distribution of FE in a parabolic strain potential has been noted by several authors.[18,30]

Of more interest is the change in spatial distribution at the phase boundaries. The temperature dependence of the spatial full width at half maximum (FWHM) of the spectrally integrated, strain-well luminescence is shown in Fig. 19 for four values of P_{abs}. At low temperatures and powers, the FWHM is almost temperature independent since most of the carriers have condensed into a compact sphere of EHL whose density varies little with temperature. However, as the temperature is raised, the FWHM increases dramatically, signaling the evaporation of the plasma phase. Once the gas phase dominates, we expect

$$\text{FWHM} = 1.67(k_B T/\alpha)^{1/2} \tag{5.1}$$

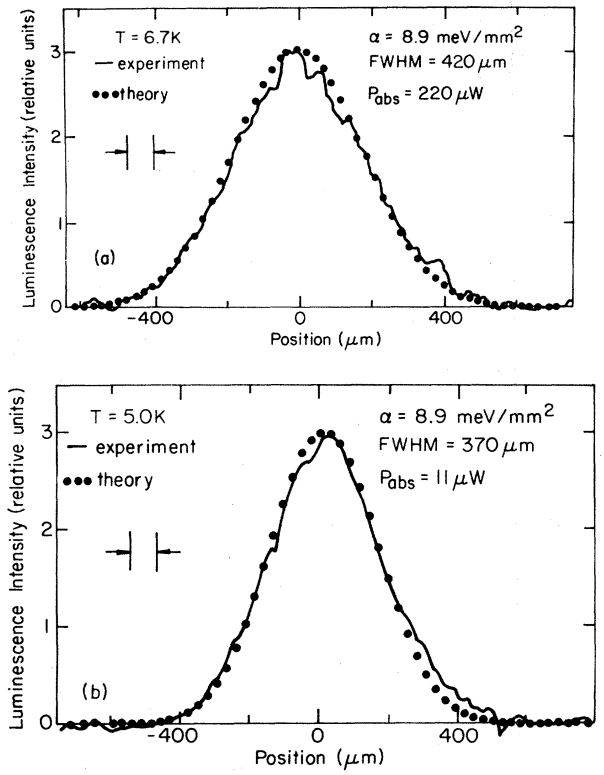

FIG. 18. Energy-integrated, recombination-luminescence intensity at (a) 6.7 and (b) 5.0 K vs position measured from the center of the strain well. The effective width of the slit that is scanned across the image of the strain well is shown in the figure. The solid circles represent a fit calculated with Eq. (4.1) for $\alpha=8.9$ meV/mm^2.

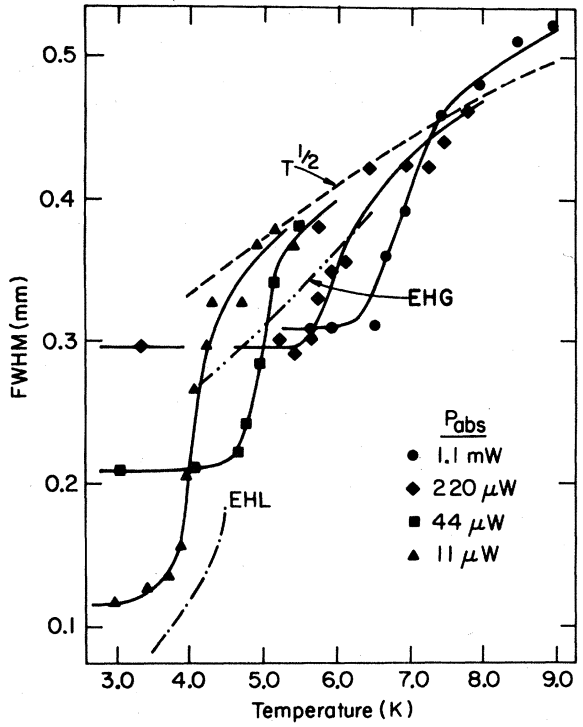

FIG. 19. Spatial FWHM of the energy-integrated luminescence vs temperature. Four series of measurements, made at constant absorbed photoexcitation power P_{abs} while the temperature was varied, are shown. At higher temperatures, the FWHM $\propto T^{1/2}$ as expected for FE in a parabolic potential well. The dotted-dashed lines labeled EHL and EHG are the calculated FWHM of these phases at their respective low-density phase boundaries. These curves were calculated with the simplifying assumptions that a uniform sphere EHP exists in the strain well just below the transition temperature, and that this sphere entirely evaporates at a single temperature determined by the FE pressure in the strain well. Note that the point at which the measured FWHM start to rapidly expand (at fixed P_{abs}) is in reasonable agreement with the calculated curves.

from Eq. (4.1). Equation (5.1) is plotted in Fig. 19 for $\alpha=8.9$ meV/mm^2. We could not follow the expansion of the FE gas very far up in temperature due to the rapid decrease in luminescence intensity, the result of the rapid decrease of FE lifetime with increasing temperature reported previously.[15]

At higher P_{abs}, the strain well contains more photoexcited carriers. This, of course, causes the radius of the EHL sphere to be larger. In addition, the mean e-h density is greater, which causes the transition to occur at a higher temperature. Note that for P_{abs} equal to 200 μW and 1.1 mW, the region of rapid volume expansion occurs well above the LG critical temperature providing additional evidence of a second phase transition extending well above 4.5 K. However, since this transition occurs by moving the interface continuously toward the center of the strain well, the spatial expansion is broadened in temperature. A proper calculation of the variation of pressure with radius cannot be done at present, since it requires knowing the equation of state of all three phases.

To make a connection between the spatial data and the phase diagram shown in Fig. 17, we assume that the pressure is actually constant throughout the well. Then, all the FE in the well would condense at a single temperature into a uniform sphere of plasma. The FWHM of this plasma sphere is related to its equilibrium density n_0 and the total number N_x of FE that were in the strain well prior to condensation,

$$\text{FWHM} = 0.877(N_x/n_0)^{1/3} . \tag{5.2}$$

As described in Sec. IV, N_x was determined by the FE luminescence intensity at the onset of EHL condensation. Superimposed on Fig. 19, we have shown the FWHM at threshold calculated from Eq. (5.2) for the EHL (dotted-dashed) and EHG (dotted-dotted-dashed) phase-boundary densities shown in Fig. 17. Of particular significance is that the EHL condensation curve increases rapidly with temperature above 4 K, in agreement with spatial data, and reflects the LG critical point at $T_{LG}=4.5$ K. The calculated EHG condensation curve lies above the observed knee in the spatial-expansion data, which very likely reflects the inappropriateness of the constant-pressure model at higher temperatures and for the compressible EHG phase. However, the substantial agreement with the spectral data of Sec. III already provides additional evidence for a LG critical temperature at 4.5 K and for a line

of first-order Mott transitions continuing to higher temperatures.

By making spectrally resolved spatial measurements at 4.0 K, we obtained additional evidence corroborating our model of three concentric shells of separate phases in this temperature range. In these measurements, an image of the strain well was scanned across the entrance slit of our spectrometer; the entrance slit determined spatial resolution, and spectral resolution was determined by the combination of entrance and exit slits. At $P_{\rm abs}=230$ μW, the spatial FWHM is 120 ± 2 μm in the EHL spectral range (704.5—706 meV). In the plasma spectral regime (707—708 meV), the FWHM is distinctly larger, 130 ± 2 μm. At photon energies at about 709 meV, the spatial FWHM increases rapidly due to the surrounding cloud of FE. Spectrally resolved spatial measurements made at a sufficiently low photoexcitation power, so that only FE are present in the strain well, prove that the FE cannot be responsible for the observed increase in the spatial FWHM observed between 707 and 708 meV. These results provide evidence for a core of EHL in the strain well at $P_{\rm abs}=230$ μW, surrounded by a thin shell of EHG, which in turn is surrounded by a FE gas.

Although our inadequate understanding of the equation of state of the dense *e-h* phases prevents a direct determination of the phase diagram from the spatial data alone, we have obtained strong corroborating evidence for the phase diagram calculated from the spectral measurements of Sec. III. This corroboration of spectral measurements by spatial measurements was a unique feature of our experiment over previous investigations of the phase diagram of photoexcited semiconductors.

VI. THEORETICAL CONSIDERATIONS OF THE MOTT TRANSITION

Kosterlitz[32] has shown that a Mott transition cannot occur at a nonzero temperature in a classical, three-dimensional (3D) Coulomb gas; instead, the gas will always have a finite conductivity. Of course, a classical model neglects such important quantum effects as the exciton bound state. These effects, however, would become increasingly less important as the density of the Coulomb gas is lowered. In particular, the ratio of exciton density n_x to uncorrelated *e-h* pair density n_0 is[33]

$$n_x/n_0 \sim n_0 T^{-3/2}\exp(-E_x/k_B T) , \tag{6.1}$$

which vanishes as the total carrier density approaches zero (E_x is the exciton binding energy).

Because the classical approximation gives an accurate description of the Coulomb gas at sufficiently low densities for $T>0$ K, Kosterlitz's result demonstrates that the Mott transition in 3D does not represent a universal change in symmetry. In other words, it is always possible to proceed from any point on the phase diagram to any other point without going through a phase transition. For instance, on the low-density (FE gas) side of the phase diagram, it is possible to get to the high-density (EHL) side by first lowering the density of the gas at constant temperature so that the excitons will be ionized due to entropy considerations without a phase transition. Next, the temperature can be raised well above E_x/k_B; then, the density of the Coulomb gas can be increased without the formation of excitons. Finally, the temperature can be lowered again so that we end up on the high-density side of the phase diagram. No phase transition occurs while the temperature is being lowered, since the Coulomb gas was fully ionized and will remain so in the EHL phase. Thus the Mott transition does not require the breaking of any universal symmetry, which rules out the existence of a line of second-order phase transitions. Instead, the Mott transition, if one occurs in the 3D Coulomb gas, must necessarily be a line of first-order phase transitions terminating at a critical point at temperature $T_{\rm Mott}$ and density $n_{\rm Mott}$.

We can estimate the location of the critical point by assuming that $n_{\rm Mott}$ is sufficiently small that both the EHG and FE phases obey MB statistics. Let n_x and n_0 be the equilibrium densities of the FE and the EHG, respectively, and the total density be

$$n=n_x+n_0 . \tag{6.2}$$

The free energy per *e-h* pair may be expressed as

$$F=(n_xF_x+n_0F_0)/n=(1-c)F_x+cF_0 , \tag{6.3}$$

where F_x and F_0 are the free-energy contributions of the FE and the EHG, respectively, and the concentration of EHG, $c=n_0/n$. If we treat the FE as an ideal gas, then F_x will be[34]

$$F_x(n_x,T)=E_g-E_x+k_BT[\ln(Q_xn_x)-1] , \tag{6.4}$$

where E_g is the band-gap energy and Q_x is the exciton quantum volume,

$$Q_x=\frac{1}{\nu_x}\left[\frac{2\pi\hbar^2}{k_BTm_{dx}}\right]^{3/2} . \tag{6.5}$$

Here ν_x is the exciton degeneracy and m_{dx} is the density-of-states mass.

Balslev[35] has expressed $F_0(n_0,T)$ as

$$F_0(n_0,T)=E_g+k_BT[\ln(n_0^2Q_eQ_h)-2] -E_x[n_0/N_{\rm DH}(T)]^{1/2} , \tag{6.6}$$

where Q_e and Q_h are defined in analogy to Q_x and $N_{\rm DH}$ is the DH density,

$$N_{\rm DH}(T)=[(1.19)^2k_BT/16\pi E_x]a_x^{-3} , \tag{6.7}$$

expressed in terms of the exciton radius a_x. Balslev obtained Eq. (6.6) by fitting the plasma band-bottom energy $E_{\rm BB}^{\rm EHG}$ (calculated[27] within MB statistics) with a simple $n_0^{1/2}$ density dependence. Note that Eqs. (6.4) and (6.6) assume that there is no interaction between the two species. While this cannot be exactly true, our experimental observations and those of Balslev and Furneaux[9] and also theoretical calculations,[27] indicate that the shift in E_x due to screening by the EHG is compensated by a corresponding shift of $E_{\rm BB}^{\rm EHG}$.

We now calculate $T_{\rm Mott}$ by requiring the first three derivatives of the free energy with respect to c in Eq. (6.3) to be zero. This is equivalent to a Landeau theory in which the leading power of an expansion of F is fourth order at $T_{\rm Mott}$. The requirement

$$\left.\frac{\partial^2 F}{\partial c^2}\right|_{c=c_c}=0 \text{ and } \left.\frac{\partial^3 F}{\partial c^3}\right|_{c=c_c}=0 \tag{6.8}$$

gives $c_c=0.4706$ and

$$n_c=22.1(T/T_0)N_{\rm DH}\ , \tag{6.9}$$

where $T_0=E_x/k_B$. The first derivative takes the form

$$\frac{\partial F}{\partial c}=E_x+k_BT\left[-\ln\left[\frac{\nu_e\nu_h}{\nu_x^2}\right]\left[\frac{(m_{de}m_{dh})^{1/2}}{m_{dx}}\right]^3 +2\ln\frac{T}{T_0}+\ln(N_{\rm DH}Q_x)-2.61\right]. \tag{6.10}$$

When the first derivative is also set equal to zero, we obtain

$$T_{\rm Mott}=5.4 \text{ and } n_{\rm Mott}=3.4\times10^{15}\ , \tag{6.11}$$

in units of K and $\rm cm^3$, respectively, using the appropriate parameters for Ge(1:2): degeneracy factors $\nu_e=2$, $\nu_h=4$, and $\nu_x=4$; density-of-state masses $m_{de}=0.22m_0$, $m_{dh}=0.088m_0$, and[22] $m_{dx}=0.415m_0$ (m_0 is the bare electron mass); and exciton binding energy[36] $E_x=2.65$ meV. The results indicated in Eq. (6.11) should be compared with the experimental values: $T_{\rm Mott}=6.5$ K and $n_{\rm Mott}=8\times10^{15}$ $\rm cm^{-3}$. The agreement is quite good considering the simplicity of our model.

VII. CONCLUSION

In this paper we have exploited the quasiequilibrium of strain-confined carriers in Ge to explore the phase diagram. The most significant feature is the identification of a line of Mott transitions which occur separately from and at lower densities than the LG transition. In particular, above 3.7 ± 0.2 K, which we identify as the triple-point temperature, excess luminescence intensity is observed at energies between the typical FE and EHL luminescence lines. This excess luminescence can be well described by the spectrum calculated for an EHG. The density of the EHG could be determined from the position of the EHG line relative to the chemical potential of the system which is fixed by the EHL line, and independently from the shift in band-bottom energy. The two values are in excellent agreement. Densities for the EHL and the EHG could be obtained from the spectroscopic data up to the LG critical temperature of 4.5 ± 0.2 K. Above this temperature, upper bounds on the EHG densities could be estimated along the Mott phase boundary up to the Mott critical temperature of 6.5 ± 0.5 K. Measurements of the actual spatial distribution of photoexcited electrons and holes confirm that sharp changes in density continue to temperatures substantially above the LG critical temperature, further evidence of a separate Mott transition. Good quantitative agreement was found between the density changes observed and those calculated from spectral analysis providing support for the proposed phase diagram.

We have also considered inhomogeneous strain broadening and the existence of excitonic complexes, but have shown them to be inadequate explanations of our data. The excess luminescence above 3.7 K was much narrower than expected[12] for excitonic complexes. In addition, we found the onset of the excess luminescence to be too abrupt with increasing density to be explainable by excitonic complexes.

We note that the apparent small density difference between the FE and EHG phases suggests that the Mott transition is only weakly first order. In fact, an alternate explanation of our data is that the Mott transition, above the LG critical temperature, is actually continuous. However, we believe that the narrowness of the transition in both temperature and laser power above T_{LG}, the sharp spatial contraction that continues to occur above $T_{\rm LG}$ and the observation of FE and EHG coexistence in the spectral data up to 6.5 K, all strongly favor the first-order phase-transition interpretation.

Another interesting result of our analysis is that the density of the EHG along the Mott phase boundary increases with increasing temperature. This feature is not present in most of the theoretical studies on the Mott transition of excitons.[2–4] However, there is one recent theoretical study[35] which indicates this possibility. The observed effect implies that correlations between the electrons and holes must play a strong role in the EHG. Further experiments and a greater theoretical understanding will be necessary to appreciate these effects.

ACKNOWLEDGMENTS

We gratefully acknowledge fruitful comments by Professor P. Nozières. This work was supported in part by the National Science Foundation under a Materials Research Laboratories Program Grant No. DMR-80-20250. During the writing of this paper, L. J. Schowalter was employed by the General Electric Company.

APPENDIX: SHIFT OF THE BAND BOTTOM WITH DENSITY

We consider here an EHP whose density of e-h pairs is n. We will write the free energy per e-h pair as

$$F(n,T)=F_K+F_{xc}\ , \tag{A1}$$

where F_K is the free energy of a system of noninteracting electrons and holes, while F_{xc} is the resulting free energy from the Coulomb interaction. The principal explicit temperature dependence of F_{xc} will come from plasmon excitations which will, however, be very small if $\hbar\omega_{\rm p}\gg kT$. This certainly is true for the density and temperature range of interest to us which suggests ignoring the temperature dependence of F_{xc} and writing it only as a sum of the ground-state exchange and correlation energies,[3]

$$F_{xc}(n,T)=E_{\rm exch}(n)+E_{\rm corr}(n)\ . \tag{A2}$$

Vashishta *et al.*[26] have calculated the exchange and correlation energy for Ge in the high stress limit. In order to obtain a simple expression, we have fitted their results to a power law (in units of meV),

$$E_{\rm exch}+E_{\rm corr}=-(6.18\times10^{-4})n^{0.243}\ , \tag{A3}$$

in the range $1\times10^{15}<n<8\times10^{16}$ $\rm cm^{-3}$. While we were

not working in the high stress limit (which is >800 MPa), Kirczenow and Singwi[37] have shown that the exchange plus correlation energy is not affected significantly by stress.

The chemical potential μ of the EHP can be calculated from the free energy per *e-h* pair,

$$\mu=\frac{\partial(nF)}{\partial n}=\frac{\partial(nF_{xc})}{\partial n}+\frac{\partial(nF_K)}{\partial n} . \tag{A4}$$

If we can treat the many-particle interactions as resulting in a renormalized band structure, then the band-bottom energy E_{BB} as a function of density will be given as

$$E_{BB}(n)=\partial[nF_{xc}(n)]/\partial n . \tag{A5}$$

Thus with Eq. (A3), we obtain (in units of meV)

$$E_{BB}(n)=-(7.68\times10^{-4})n^{0.243} . \tag{A6}$$

On the other hand, Zimmermann *et al.*[27] have treated a plasma in the limit of MB statistics. This should be valid at temperatures well above the EHP's Fermi temperature. Their results can be fit[35] to

$$E_{BB}(n,T)=-[2.3n/N_{DH}(T)]^{1/2}E_x , \tag{A7}$$

where E_x is the exciton binding energy and N_{DH} is the DH density defined as[4]

$$N_{DH}=0.0282k_BTE_x^{-1}a_x^{-3} . \tag{A8}$$

Unfortunately, these two results leave unanswered the question of how to extrapolate from the high-density limit [Eq. (A6)] to the low-density results [Eq. (A7)]. We have proceeded, nonetheless, in a very *ad hoc* fashion. The only requirements we put on the extrapolation function was that it go smoothly from one limit to the other and that $|E_{BB}|$ monotonically increased with density, and that the transition between the two regimes at a given density occur at a temperature proportional to the Fermi temperature. A function that met these requirements was (in units of meV)

$$E_{BB}=-12.0[p^{0.243}f(3500T^{-3/2}p,T) +11.1(p/T)^{1/2}f(-3500T^{-3/2}p,T)] , \tag{A9}$$

where

$$p=n(5.55\times10^{-18}\text{cm}^{-3}) \tag{A10}$$

and

$$f(x,T)=\{\exp[(-x+1/x)\sqrt{T}]+1\}^{-1} . \tag{A11}$$

The transition from the high density limit to the MB results is centered about $T=1.5T_{Fh}$ where T_{Fh} is the hole Fermi temperature. In Fig. 6, E_{BB}, as determined by Eq. (A9), is plotted versus n for several different temperatures.

---

*Present address: General Electric Corporate Research and Development Center, P.O. Box 8, Schenectady, NY 12301.

[1]L. D. Landau and G. Zeldovich, Acta Physicochim. URSS 18, 194 (1943) [translation can be found in *Translations of the Collected Papers of L. D. Landau,* edited by D. ter Haar (Pergamon, Oxford, 1965), p. 380].

[2]N. F. Mott, Philos. Mag. B 37, 377 (1978).

[3]T. M. Rice, in *Solid State Physics,* edited by H. Ehrenreich, F. Seitz, and D. Turnbull (Academic, New York, 1977), Vol. 32, p. 1 and references therein.

[4]N. F. Mott, *Metal-Insulator Transitions* (Taylor and Francis, London, 1974).

[5]J. C. Hensel, T. G. Phillips, and G. A. Thomas, in *Solid State Physics,* edited by H. Ehrenreich, F. Seitz, and D. Turnbull (Academic, New York, 1977), Vol. 32, p. 87, and references therein.

[6]W. Miniscalco, C.-C. Huang, and M. B. Salamon, Phys. Rev. Lett. 39, 1356 (1977).

[7]J. Shah, M. Combescot, and A. H. Dayem, Phys. Rev. Lett. 38, 1497 (1977).

[8]G. A. Thomas, J. B. Mock, and M. Capizzi, Phys. Rev. B 18, 4250 (1978).

[9]I. Balslev and J. E. Furneaux, Solid State Commun. 32, 609 (1979).

[10]T. M. Rice, *Proceedings of the 12th International Conference on the Physics of Semiconductors, Stuttgart* (Teubner, Stuttgart, 1974), p. 23.

[11]M. Combescot, Phys. Rev. Lett. 32, 15 (1974).

[12]G. A. Thomas and T. M. Rice, Solid State Commun. 23, 359 (1977).

[13]M. Greenstein and J. P. Wolfe, Solid State Commun. 33, 309 (1980).

[14]R. S. Markiewicz, J. P. Wolfe, and C. D. Jeffries, Phys. Rev. B 15, 1988 (1977).

[15]L. J. Schowalter, F. M. Steranka, M. B. Salamon, and J. P. Wolfe, Solid State Commun. 37, 319 (1981).

[16]P. L. Gourley and J. P. Wolfe, Phys. Rev. Lett. 40, 526 (1978).

[17]Boule 145 from E. E. Haller of Lawrence Berkeley Laboratory.

[18]J. P. Wolfe, R. S. Markiewicz, S. M. Kelso, J. E. Furneaux, and C. D. Jeffries, Phys. Rev. B 18, 1479 (1978).

[19]R. P. Ries and B. K. Moore, Rev. Sci. Instrum. 41, 996 (1970).

[20]I. Balslev, Phys. Rev. 143, 636 (1966).

[21]S. M. Kelso, Ph.D. thesis, University of California, Berkeley, 1979; S. M. Kelso, Phys. Rev. B 25, 1116 (1982); table of values kindly supplied in private communication.

[22]B. J. Feldman, H.-H. Chou, and G. K. Wong, Solid State Commun. 24, 521 (1977).

[23]J. E. Furneaux, Ph.D. thesis, University of California, Berkeley, 1979; J. C. Culbertson and J. E. Furneaux, Phys. Rev. Lett. 49, 1528 (1982).

[24]R. M. Westervelt, J. L. Staehli, and E. E. Haller, Phys. Status Solidi B 90, 557 (1978).

[25]R. S. Markiewicz and S. M. Kelso, Solid State Commun. 25, 275 (1978); S. M. Kelso, Phys. Rev. B 26, 591 (1982).

[26]P. Vashishta, P. Bhattacharyya, and K. S. Singwi, Phys. Rev. B 10, 5108 (1974).

[27]R. Zimmerman, K. Kilimann, W. D. Kraeft, D. Kremp, and G. Ropke, Phys. Status Solidi B 90, 175 (1978).

[28]H.-H. Chou and G. K. Wong, Phys. Rev. Lett. 41, 1677 (1978).

[29]L. J. Schowalter, Ph.D. thesis, University of Illinois, Urbana-

Champaign, 1981.
[30]P. L. Gourley and J. P. Wolfe, Phys. Rev. B 20, 3319 (1979); V. D. Kulakovsky and V. B. Timofeev, Zh. Eksp. Teor. Fiz. Pis'ma Red 25, 487 (1977) [JETP Lett. 25, 458 (1977)]; I. V. Kukushkin, V. D. Kulakovsky, and V. B. Timofeev, J. Lumin. 24, 393 (1981).
[31]D. Kremp, W. Ebeling, and W. D. Kraeft, Phys. Status Solidi B 69, K59 (1975).
[32]J. M. Kosterlitz, J. Phys. C 10, 3753 (1977).
[33]See, for example, F. Reif, *Fundamentals of Statistical and Thermal Physics* (McGraw-Hill, New York, 1965), p. 324.
[34]See, for example, C. Kittel, *Thermal Physics* (Wiley, New York, 1969).
[35]I. Balslev, Phys. Status Solidi B 101, 749 (1980).
[36]B. J. Feldman, H.-H. Chou, and G. K. Wong, Solid State Commun. 26, 209 (1978).
[37]G. Kirczenow and K. S. Singwi, Phys. Rev. B 19, 2117 (1979).